

THE NATURE OF TURBULENT BOUNDARY LAYER SUB-CONVECTIVE PRESSURE FLUCTUATIONS

Shishir Damani, Eric Totten, Humza Butt, Bhavika Sharma, William J. Devenport, Todd K. Lowe

Department of Aerospace and Ocean Engineering
Virginia Polytechnic Institute and State University
Blacksburg, Virginia, USA - 24060

shishirdamani@vt.edu, erict1@vt.edu, hbutt@vt.edu, bhavika@vt.edu, wdevenpo@vt.edu, kelowe@vt.edu

ABSTRACT

Sub-convective wall pressure fluctuations, which are known to coexist with superstructures in turbulent boundary layer flows, are discussed with implications for wall pressure modeling of surface flow noise generated by smooth and rough surfaces. Discrepancies in past measurements of the sub-convective pressure spectrum have been due to limitations in measurement techniques. The study presented here identifies an approach towards accurately measuring the sub-convective pressure fluctuations and quantifies the spectrum at low-wavenumbers for a single flow condition for two surfaces. Correlations between different sensors suggests smaller scales in rough walls than smooth walls. The sub-convective pressure spectrum levels observed are about 35 dB below the convective pressure fluctuations for smooth walls while 15-20 dB for rough walls. A non-wavenumber-white dependence is observed at higher frequencies for smooth walls while a wavenumber-white behavior is depicted for rough walls. Comparisons with a modified Corcos wall pressure model show deviations in convective ridge roll-off and levels in the sub-convective regime at various frequencies. A convection velocity dependency is observed for both smooth and rough walls with higher prominence in the latter case.

INTRODUCTION

The turbulent boundary layer wall pressure wavenumber-frequency spectrum for a homogeneous, zero-pressure gradient, high Reynolds number flow can be divided into three regions: i) convective ridge, ii) sub-convective regime and iii) supersonic cone. There have been large dissimilarities identified between well-known wall pressure models and measured data for the sub-convective and supersonic regions (Graham, 1997; Blake, 2017). Additionally, past measurements are difficult to compare with since they are mostly available for a few discrete wavenumber and frequency points due to the limitations in measurement approaches. Amongst models, there are variations at low-wavenumbers due to different theories behind their description and scarcity in data (Graham, 1997). Furthermore, the quantification of pressure fluctuations has been very limited for practical flows, such as those with surface roughness. When surface roughness is introduced into a turbulent boundary layer, the wall-pressure frequency spectrum changes quite drastically (Catlett *et al.*, 2021). Many measurements of the single-point wall pressure spectrum have been made for fully rough turbulent boundary layer flows, and there has been success in modeling these spectra across wide frequency ranges (Blake, 2017; Catlett *et al.*, 2021). However, reliable

measurements and models of the continuous wavenumber-frequency spectrum for rough wall turbulent boundary layer flows are required if we are to understand the parts of the pressure field that contribute most to structural vibration and noise.

In both smooth and rough wall turbulent boundary layer flows, pressure fluctuations pertaining to the sub-convective regime are primarily responsible for generating interior and exterior noise by coupling with the primary structural modes of the surface (Abtahi *et al.*, 2024). The major contributing factor to the disparities seen between various wall pressure models can be attributed to challenges in measuring the sub-convective pressure fluctuations distinctly. This is a two-fold problem. First, due to the weak nature of sub-convective pressure fluctuations, it is difficult to distinguish them from the dominant convective fluctuations, and the acoustic contamination of the facility. Second, limitations in wall pressure sensing technology result in measurements that suffer from spatial aliasing and poor signal-to-noise ratio in the sub-convective regime.

Recently, there have been developments on wall pressure sensing involving sub-resonant acoustic cavities covered with a Kevlar scrim to measure boundary layer pressure fluctuations with better signal-to-noise ratios (Damani *et al.*, 2022a). Such cavity based-sensors have minimal disturbance to the flow characteristics (Damani *et al.*, 2022b). These Kevlar covered cavities provide area averaging of surface pressure fluctuations but were found to have membrane effects making it difficult to control the averaging. An extension of this technology, recently tested by Damani *et al.* (2024), uses acoustic resonating cavities with a rigid porous interface made up of the same 3D-printed material (Accura 60) as the cavities perforated with a designed distribution of small pores. This avoids membrane-effect complications in sensor response, allows for the embedding of sensors in both smooth and rough walls, and provides additional freedom in sensor shape and area sensitivity. This in turn allows for closer placements between adjacent sensors, hence pushing aliasing to higher wavenumbers. In the current study, measurements have been obtained for a continuous range of wavenumbers and frequencies, revealing a well-defined separation between the various regions in the wavenumber-frequency spectrum. The measurements were taken using an array of evolved sensors as described in Damani *et al.* (2024) over near zero-pressure gradient boundary layer flows on smooth and rough walls. A quantitative comparison is performed between the characteristics of the sub-convective wall pressure for smooth and rough walls for a single flow condition.

EXPERIMENTAL SETUP

Measurements were taken in the aerodynamic configuration of the Virginia Tech Stability Wind Tunnel. A detailed description of the test section is given in Damani *et al.* (2022b). Test boundary layers were formed on the 1.85 m wide port-side wall of the test section, and initiated at a 3.18 mm high trip strip located 3.58 m upstream of the test section entrance. The test section is parallel sided and was empty except for a 0.914 m chord NACA 0012 airfoil placed at the center of the test section with its span parallel to the port wall, and its leading edge 3.22 m downstream of the test section entrance and 0.925 m away from the test wall. For the measurements presented here, the airfoil was held at zero angle of attack so that pressure gradients along the test wall remained small. Measurements were made at free-stream flow speeds close to 23 m/s. Precise test conditions (including residual pressure gradients and boundary layer properties) are given in Table 1.

Two surface finishes were studied: a smooth wall and a rough wall. The smooth wall surface consisted of a factory standard aluminum 6061 surface finish while the rough wall was comprised of staggered cylindrical roughness elements arranged according to Figure 1. The rough surface was applied starting at the test section entrance. The rough surface dimensions were selected in order to tile seamlessly between panels in the facility, and have been investigated extensively both experimentally and numerically by Vishwanathan *et al.* (2023); Mulchandani *et al.* (2021). The effective sand-grain roughness to geometric roughness height ratio for this surface is $k_s/k_g = 1.6$ (Vishwanathan *et al.*, 2023). For the conditions of the present study (Table 1) the roughness Reynolds number was found to be $k_s^+ \approx 210$, indicating a fully rough flow.

Measurements of the spanwise-homogeneous mean velocity profiles of the boundary layers, supplementing those made by Vishwanathan *et al.* (2023), were obtained using a Pitot-static rake. These profiles, Figure 1, indicate boundary layer thicknesses of 69.7 mm and 94.0 mm at friction Reynolds numbers of 3320 and 6130, respectively for the smooth and rough flows. Note that the Clauser parameter value indicates a small favorable pressure gradient for both cases.

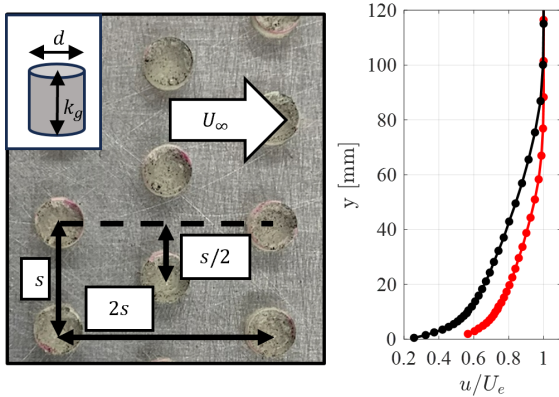


Figure 1: *Left*: Staggered cylinder rough wall dimensions $s = 6.93$ mm, $k_g = 2$ mm, $d = 3.14$ mm; *Right*: Boundary boundary layer profile for smooth (—) and rough wall (—).

Sub-Convective Pressure Sensing Arrays

The wall pressure measurements were conducted using an array of in-house designed sensors. The smooth and rough wall arrays were designed based on model predictions of the wall pressure wavenumber-frequency spectrum they would measure. These predictions used the modified Corcos

Table 1: Boundary layer parameters for smooth and rough walls. Note on dimensions: length in *mm*, velocity in *m/s* and viscous scale in μm .

Parameters	Smooth	Rough
Edge Velocity (U_e)	22.73	23.86
Boundary Layer Thickness (δ)	69.7	94.0
Displacement Thickness (δ^*)	10.4	19.5
Viscous Scale (ν/u_τ)	24.0	15.3
Friction Re (Re_τ)	3320	6130
Momentum Thickness Re (Re_θ)	9860	16970
Clauser Parameter (β)	-0.31	-0.16
Mach Number (M)	0.065	0.067

(Hwang *et al.*, 2003) model for the wavenumber spectrum, the Goody (Goody, 2004) frequency spectrum, and employed the wavenumber transform of the spatial sensitivity function of the sensor to arrive at the predicted measured spectrum. The spatial sensitivity function of the sensors was assumed to be a summation of uniformly weighted delta functions distributed over space, each located at a pore location. We are assuming here that at sub-resonant frequencies (below which no acoustic modes are possible in the sensor cavities), the cavities behave as simple multi-pore Helmholtz resonators, equally sensitive to the pressure presented at each (identical pore). Bias errors were evaluated between the predictions and a spanwise averaged form of the spectrum for a pores distribution. On varying the pores distribution over space, the errors revealed sensitivity towards arrangement of pores along the flow direction and performed better for uniform distributions. Errors were mainly studied in the sub-convective regime ranging from 0 – 200 rad/m and 100 – 3000 Hz. Based on manufacturing capabilities and error maps from the modeling approach, an array design was chosen for both surfaces. The surface area interacting with the flow for each sensor was chosen based on a baseline flow condition in the facility and the wavenumber-frequency range of interest. This has been documented in detail by Damani *et al.* (2024).

The smooth wall array consisted of 80 sensors, each with a rectangular sensing area extending 5 mm in the streamwise direction and 50 mm spanwise. The sensors are placed in a streamwise row, as closely as possible (5.5 mm center-to-center distance). Each sensor (Figure 2a) used a lofted design for the cavity to accommodate the close sensor spacing. Each sub-resonant cavity communicated the wall pressure to a G.R.A.S. Type 40PH-S5 1/4" microphone at its base through 80, 0.4 mm diameter pores drilled into the rigid 1.1 mm thick interface. The pores were laid out in a rectangular grid with 2.5 mm spacing in the spanwise direction and 1.375 mm in the streamwise direction, as can be seen in Figure 2a. Adjacent sensors were oriented in an alternating fashion to avoid microphone overlap (Figure 2b). The array had a maximum sensor separation of 434.5 mm, equivalent to 6.2δ . Photographic views of the manufactured smooth wall array are shown in Figure 2c and 2d. The rough wall array had a very similar construction to the smooth wall array except that the flow interface included hollow roughness elements so that pores could be drilled both through the elements and the substrate portions of the surface. For the rough surface, the pore spacing

changed to 1.732 mm in both directions. The cavities were increased in size and the spacing between consecutive sensors was 6.93 mm, to accommodate the periodicity of the roughness elements on the surface. The rough wall array consisted of 64 sensors covering a maximum separation of 436.4 mm, equivalent to 4.6δ . A photographic view of the manufactured rough wall array is shown in Figure 2e.

Both arrays were calibrated in an anechoic chamber with a cut-off frequency of 100 Hz. A standard microphone calibration procedure was used involving reference pressure measure-

ments and measurements with the array of sensors using an omnidirectional source (B&K Type 4292-L). The HBK Type 4144/4145 1" (23.7 mm) microphones were utilized for the reference measurements. The source field function from the reference measurement was used to back out individual sensor response on the array. This also required time delay calculations due to differences in sensor and reference microphone locations. The dynamic response was smoothed using curve fitting to reduce any uncertainty due to the setup including scattering from the mounting structure.

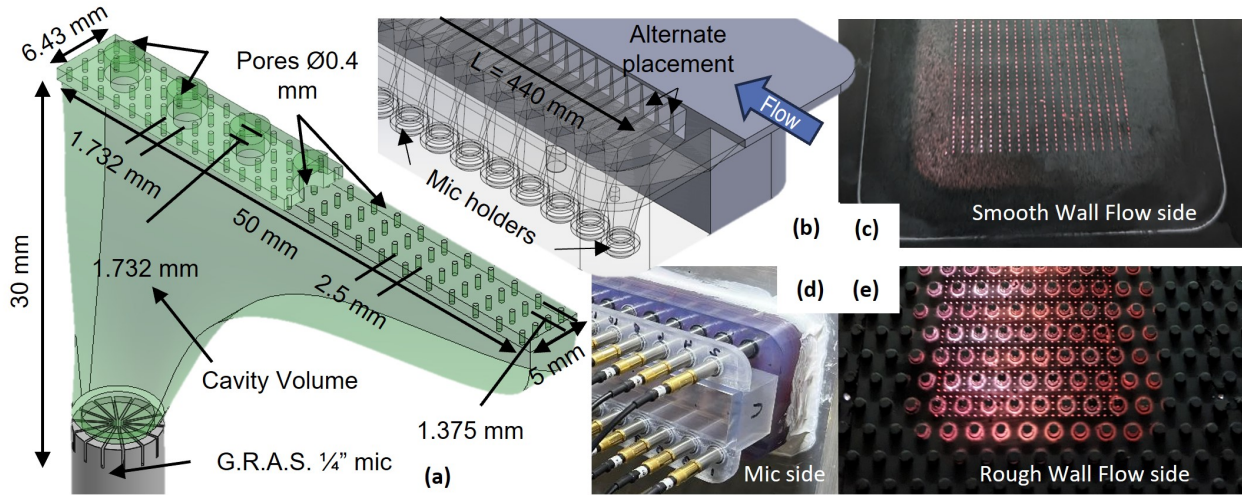


Figure 2: (a) CAD profile of sensor cavity shown for smooth (*right*) and rough (*left*) walls; (b) CAD sectional view of the arrangement of the sensors in a linear pattern; (c) Photographic view of the smooth wall array of sensors from the flow side; (d) View from the back side of the arrays showing the microphones; (e) Rough wall array from the flow side.

Two adjustments to the anechoic chamber calibrations were necessary for the smooth wall array. First, phase calibrations showed a localized non-linear feature around 2 kHz believed to be due to imperfections in the calibration sound field. This was corrected by substituting a linear phase variation based on the measured calibration at surrounding frequencies. Second, magnitude calibrations were adjusted to account for grazing flow effects (Fritsch *et al.*, 2021). Measurements of the pointwise wall pressure spectrum made with the HBK 1/8" pinhole microphones, represented as an analytic function obtained by fitting a Goody-like spectrum model, were used to infer the form of the autospectrum averaged over the 50×5.5 mm area of the sub-resonant sensors. This was then used to correct for residuals from the anechoic calibrations. This approach was chosen as it was not possible to directly measure the wall pressure from the sensor without knowing its area averaging capability and the grazing-flow dependence. In the future, this will be done by quantifying area sensitivity of such sensors using measurements or FEA simulations.

Measurements were made using a 16-bit data acquisition system with simultaneous 128 channel sampling. The time duration of sampling was chosen to be 320 seconds for the smooth wall measurements with a sampling rate of 25600 Hz after a coherence convergence study which yielded enough averages (5000) to resolve turbulent pressure coherence levels between sensor pairs down to 0.0003 (-35 dB), and in some cases, significantly lower. The rough wall data acquisition was made for 256 seconds at a sampling rate of 25600 Hz. Long measurement times were used to capture the scales associated with superstructures and to reduce uncertainty in the sub-convective (much weaker) fluctuations. The frequency spectrum was evaluated with 4096 samples per record with a

50% overlap. Surface pressure measurements were also obtained using a short array of four HBK Type 4144/4145 1" microphones (same microphones were used by Farabee & Geib (1991)) arranged linearly with a streamwise separation of 26.9 mm. This array of microphones will be referred to as the F&G array. The wavenumber-frequency spectrum levels were calculated using the difference mode described in Farabee & Geib (1991) where the auto-spectrum from each alternating microphone was subtracted while summing over all 4 microphones. This generated a scaled zero-spanwise wavenumber spectrum at a single wavenumber of π/d where $d = 26.9$ mm is the distance between the microphones. The scaling factor was $5.7 \times 10^4 m^2$ which was divided out to obtain the spectrum level. These measurements were taken to serve as a reference for the measurements shown in this study. However, it is important to note that the measurements obtained using the F&G array reflect levels for the zero-spanwise wavenumber component of the wall pressure spectrum while the array measures the spanwise averaged (over the sensor area) spectrum.

RESULTS

This section describes the statistical characteristics of the sub-convective wall pressure fluctuations over smooth and rough walls for flow conditions described in Table 1. The results are described in an increasing order of complexity starting with the autospectrum of the sensors and their comparison with existing wall pressure models, followed by the cross-correlation in the form of coherence and the wavenumber-frequency spectrum. Selective slices of the wavenumber-frequency spectrum are taken and compared with the modified Corcos model. Note that all frequency axes would be limited to the cut-off frequency of the sensor of 3500 Hz.

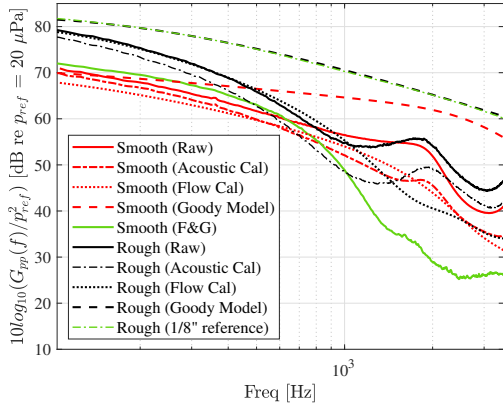


Figure 3: Autospectrum comparisons between smooth (red) and rough (black) walls. Reference measurements (green) and models are also shown.

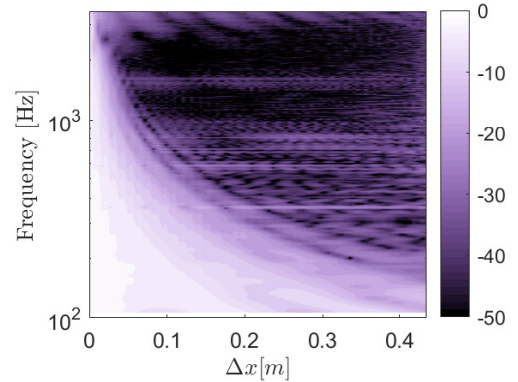
Figure 3 shows the averaged autospectrum in dB relative to $20\mu\text{Pa}$ of all sensors as-measured (solid), calibrated using acoustic calibrations (dash-dotted) and flow-based calibrations (dotted), for the flow conditions of Table 1. The smooth wall is represented using the color red. The as-measured spectrum shows a rise in levels close to 2 kHz which corresponds to the resonance of the sensor cavity. Acoustic calibrated curve (red dash-dotted) corrects for this resonance response but there is a residual bump due to flow-grazing effects. Additionally, two plots are shown for smooth wall from the F&G array (solid green) and a pointwise pressure spectrum using the Goody model (dashed red). Overall, there are variations in levels among various plots and is mainly due to differences in area over which pressure fluctuations are averaged. The pointwise pressure spectrum model has higher broadband levels due to the least area averaging. The measured pointwise levels (not shown) are higher than the Goody model closer to the reference measurement (solid green) at low frequencies. The F&G array measurements observe a steep roll-off after 600 Hz due to highest area averaging followed by an aliased bump at 1800 Hz. The agreement between the flow-based calibrations and the anechoic calibrations is within 2 dB with the exception that the flow-based calibrations suppress the residual bump. Hence, these calibrations are used for the smooth wall data in the results that follow.

The rough wall data is represented using the color black in Figure 3. This figure includes the same spectra plots as smooth wall, except the reference plot, which corresponds to pointwise pressure measurements performed using B&K Type 4138 microphones with 0.5 mm pinhole cap. The as-measured spectrum for the rough wall (solid black) shows a significant bump at the resonant frequency of the cavity just below 2 kHz. Acoustic calibrations applied to the spectrum (black dash-dotted) correct for the bump seen at the resonant frequency of the sensor, but due to effects of grazing flow, the bump is not completely removed. Flow-based calibrations applied to the spectrum (black dotted) were obtained similar to the smooth wall. However, this method has led to an over-correction of the spectrum which significantly decreased levels at high frequency, while increasing levels in the low frequency regime. This introduces an uncertainty on the order of 10 dB when using flow-based corrections, whereas the anechoic calibrations provide an uncertainty on the order of 3 dB. For this reason, only anechoic calibrations have been used in the results that follow. Further studies aim to build upon current flow-based calibrations to reduce this uncertainty through an

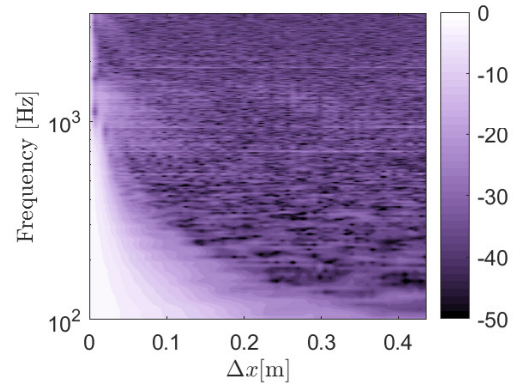
understanding of the area sensitivity over each sensor.

Figure 4a shows the surface pressure coherence for each flow as a contour map with frequency in Hz as the ordinate and streamwise separation in meters as the abscissa. As rows of equally spaced sensors, the arrays contain many sensor pairs that duplicate the same streamwise separations, particularly at smaller separations. Unlike in a conventional acoustic array, this redundancy is highly desirable since it provides further opportunity for statistical averaging and convergence. Thus coherence levels shown in these plots are averaged over these duplicate separations. The coherence spectra show a distinct decay with increasing separations, qualitatively similar to the Corcos model decaying exponential. At higher separations and frequencies the noise floor becomes apparent. It is to be noted that the levels in this region seems to be 45-50 dB below perfect coherence suggesting fluctuations $10^{-4} - 10^{-5}$ times weaker than convective fluctuations. Comparing the two cases, one can observe significant coherence beyond the length of the array (equivalent to $6 - 7\delta$) at low frequencies for the smooth wall while the rough wall shows coherence dying away just short of the array length (equivalent to only 4δ). This reflects that the spatial scales extend to further distances in the case of smooth wall while are restricted to a tighter band for rough wall. An interesting feature of Figure 4a is the existence of parallel ridges to a main region indicating a sinc (sinc/x) function behavior at specific frequencies. This behavior is a consequence of the surprising compactness of the smooth wall convective ridge in wavenumber, as will be discussed further below. This is not visible for the rough wall pressure field.

Close inspection of Figure 4a shows banding (saw-tooth behavior) at intervals of 0.011 m along the x -axis. This re-



(a) Smooth wall

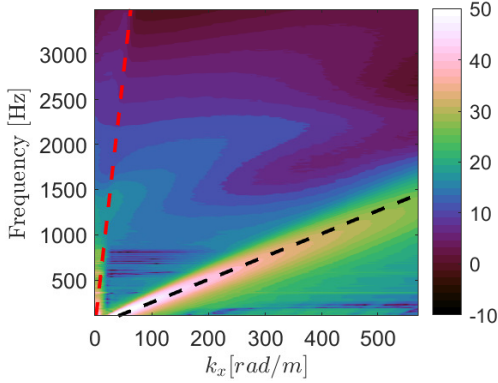


(b) Rough Wall

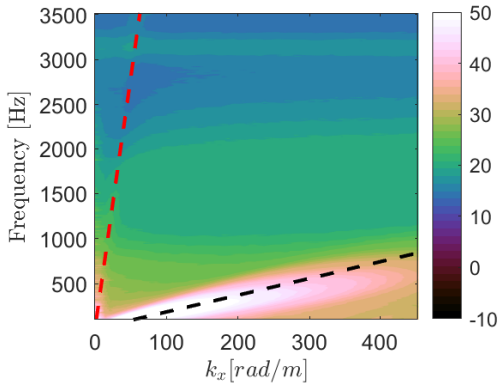
Figure 4: Average coherence between all sensors as a function of frequency and spatial separation.

sults from imperfection in the uniform area sensitivity function of the sub-resonant sensors. This results in an effective spanwise separation between the adjacent sensors, an artifact of area sensitivity slightly weighted to the microphone location. Recently, there was an attempt to quantify this area sensitivity offset using acoustic measurements and FEA analysis with COMSOL. Both techniques suggest about 5 mm of effective spanwise separation, but further investigation is needed to validate the possibility of corrections. Hence, this study will present results with no correction for this spanwise offset.

On taking a Fourier transform of the cross-spectral matrices along the spatial dimension, wavenumber-frequency spectra are generated as shown in Figure 5. The abscissa shows the wavenumber in rad/m until the Nyquist limit and the ordinate shows the frequency. The contours clearly depict the distinction between the convective ridge (centered on black dashed line) and the acoustic cone (red dashed line). The acoustic cone is prominent at lower frequencies showing the sound waves grazing the arrays. In the case of the smooth wall boundary layer, Figure 5a, a sharp decay is observed in levels as one moves away from the convective ridge to higher frequencies at a given wavenumber. A 30-35 dB drop in levels can be seen in the sub-convective portion of the spectrum compared to the convective portion. Note that the feature that runs parallel to the convective ridge originating at about 1200 Hz on the frequency axis is believed to be the result of aliasing due to the effective spanwise offset described above. Comparing model predictions (Damani *et al.*, 2024) with an effective spanwise shift to the data reveals measured levels (10-15 dB) lower than the model below the aliased region. The measured levels in the aliased region seem to show levels 10 dB above



(a) Smooth wall



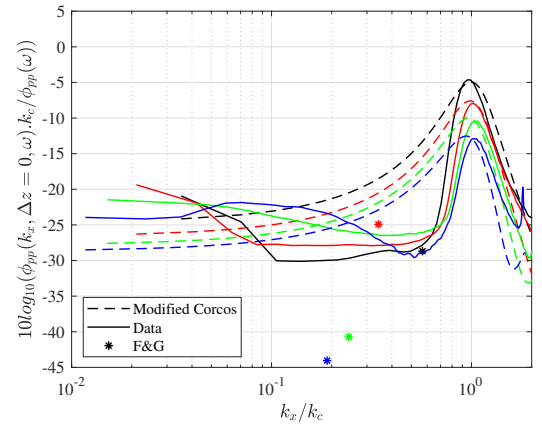
(b) Rough Wall

Figure 5: Wavenumber-frequency spectrum. (—) Acoustic line; (---) Convective line

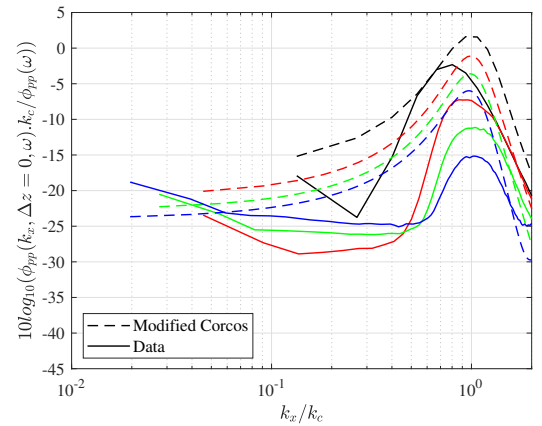
the model. Note that this discrepancy is believed to be due to the gap between the true and modeled area sensitivity of the sensor. The behavior at higher frequencies is not observed to be wavenumber white for the smooth wall case.

The rough wall wavenumber frequency spectrum has a quite different form with sub-convective levels 15-20 dB higher than those seen with the smooth wall. The convective ridge is considerably broader, and its much shallower slope is a consequence of the substantially lower average convection velocity over the rough wall ($U_c/U_e = 0.49$ for rough and 0.7 for smooth). Furthermore, the sub-convective levels outside the acoustic cone are almost wavenumber white. Spectral levels inside the cone are more than 10 dB higher than those for the smooth wall. Since background noise levels in the wind tunnel would have been similar with the smooth and rough walls, this implies that these supersonic levels represent largely uncontaminated measurements of the rough wall fluid dynamics and associated roughness noise. Note that at higher frequencies the rough wall spectral levels may include some uncertainty (≤ 5 dB) associated with uncorrected grazing flow effects (Figure 3).

A comparison between the data and the modified Corcos model (Hwang *et al.*, 2003) is shown in Figure 6 at selective normalized frequencies for the smooth and rough wall cases. These represent horizontal slices of Figure 5 normalized on the convective wavenumber and the pointwise pressure spec-



(a) Smooth wall: (—) $\omega\delta^*/U_e = 1.5$; (—) $\omega\delta^*/U_e = 2.5$;
 (—) $\omega\delta^*/U_e = 3.5$; (—) $\omega\delta^*/U_e = 4.5$.



(b) Rough Wall: (—) $\omega\delta^*/U_e = 0.5$; (—) $\omega\delta^*/U_e = 1.5$;
 (—) $\omega\delta^*/U_e = 2.5$; (—) $\omega\delta^*/U_e = 3.5$.

Figure 6: Constant frequency slices of the wavenumber-frequency spectrum.

trum. Solid lines represent the measured data and the dashed lines show the modified Corcos model evaluated at the same flow conditions as measured data. For the smooth wall, Figure 6a shows an agreement in convective peak levels for all slices between the predictions and the measurements. It is interesting to observe a difference in the behavior of convective ridge roll-off at lower wavenumbers. The data suggests for a drastic drop (with a slope approaching -20) compared to the more gradual roll-off of the model. We believe this tight constraining of the convective ridge in wavenumber is responsible for the lobed structure of the coherence spectrum in Figure 4a. The levels at lower wavenumbers also seem to be lower than the predictions from the model. Note that the levels at very low normalized wavenumbers ($k_1/k_c < 0.4$), are due to acoustics or aliased behavior (effective spanwise shift) depending on the frequency slice. Levels at single wavenumbers from the F&G array are shown using (*) symbol. Their agreement to measured data seems satisfactory for the lower frequencies but these indicate lower levels at higher frequencies. Also, Farabee & Geib (1991) recognized sub-convective levels at a single frequency of 2500 Hz, which here is in the aliased portion of the spectrum measured by the array. Figure 6b shows the results for the rough wall compared with the modified Corcos model predictions with rough wall boundary layer parameters. There is a general disagreement in the levels including the convective peak. The convective peak seems to be broader than smooth wall. The roll-offs predicted by the model seem to be different too, the roll-off rate being about half that for the smooth wall. Note that both smooth and rough wall cases show a shift in convective peak as the frequency is increased indicating a frequency dependent convection velocity. This is not captured by the model.

CONCLUSIONS

This study presents measurements of sub-convective pressure fluctuations in turbulent boundary layer flows obtained using arrays of sensors comprising of sub-resonant acoustic cavities. The cavities sample the flow pressure through designed pores in a rigid interface - an approach that can be employed with both smooth and rough walls, and that provides controlled area-averaging of the pressure signal. The arrays were used to measure surface pressure cross-spectra as a function of separation from $0.08 - 6.2\delta$ with the smooth wall, and $0.07 - 4.6\delta$ with the rough wall. The coherence shows a distinctive decay as a function of spatial separation at all frequencies with the smooth wall showing larger scales than the rough wall, relative to the boundary layer thickness. For the smooth wall, sub-convective pressure levels are about 35 dB below the convective pressures. The behavior of the spectrum seems to have non-wavenumber white nature. The rough wall shows a wavenumber-white behavior with 15-20 dB higher levels than smooth walls. Smooth wall data shows good agreement with the modified Corcos model at convective wavenumbers whereas a drastic roll-off is observed away into the sub-convective domain. This roll-off is sufficiently rapid to result in oscillatory behavior in the coherence with spatial separation. Rough walls in general show disagreement with the model while there is a consistent dependency of convection velocity on the frequency in both smooth and rough walls. In addition to contributing to the wall pressure spectrum data available at sub-convective regimes for homogeneous turbulent boundary layer flows, this study suggests a need for improvements in existing wall pressure models for both smooth and rough walls.

ACKNOWLEDGEMENTS

The authors would like to acknowledge Dr. Yin-Lu Young and the Office of Naval Research (ONR) for sponsoring this research under grant numbers N00014-20-1-2821 and N00014-22-1-2789. The authors would also acknowledge the efforts of the machine shop at the AOE department at Virginia Tech, and the staff at the VT Stability Wind Tunnel.

REFERENCES

- Abtahi, Hesam, Karimi, Mahmoud & Maxit, Laurent 2024 On the challenges of estimating the low-wavenumber wall pressure field beneath a turbulent boundary layer using a microphone array. *Journal of Sound and Vibration* **574**, 118230.
- Blake, William K 2017 *Mechanics of flow-induced sound and vibration, Volume 2: Complex flow-structure interactions*. Academic press.
- Catlett, Matthew R., Bryan, Benjamin S., Chang, Natasha, Hemingway, Hugh & Anderson, Jason M. 2021 *Modeling Unsteady Surface Pressure Auto-Spectra for Turbulent Boundary Layer Flow over Small Dense Roughness*.
- Damani, Shishir, Braaten, Erik, Szoke, Máté, Alexander, William N, Devenport, William J, Balantrapu, N Agastya, Pearce, Benjamin P, Starkey, Timothy A, Hibbins, Alistair P & Sambles, J Roy 2022a Resonator-based pressure sensor for wall pressure. In *28th AIAA/CEAS Aeroacoustics 2022 Conference*, p. 2956.
- Damani, Shishir, Butt, Humza, Banks, Jarrod T., Srivastava, Surabhi, Balantrapu, N. Agastya, Lowe, Todd & Devenport, William J. 2022b Low-wavenumber wall pressure measurements in zero-pressure gradient boundary layer flow. *AIAA SCITECH 2022 Forum*.
- Damani, Shishir, Butt, Humza, Totten, Eric, Chaware, Shreyas, Sharma, Bhavika, Devenport, William J. & Lowe, Todd 2024 The characteristics of sub-convective wall pressure fluctuations in a turbulent boundary layer. In *AIAA SCITECH 2024 Forum*, p. 1904.
- Farabee, Theodore M. & Geib, F. E. J. 1991 Measurements of boundary layer pressure fluctuations at low wavenumbers on smooth and rough walls. *NCA - Flow Noise Modeling, Measurement, and Control*.
- Fritsch, Danny, Vishwanathan, Vidya, Lowe, Todd & Devenport, William J. 2021 *The Effect of Grazing Flow on Pinhole Condenser Microphones*.
- Goody, Michael 2004 Empirical spectral model of surface pressure fluctuations. *AIAA Journal* **42** (9), 1788–1794.
- Graham, W.R. 1997 A comparison of models for the wavenumber-frequency spectrum of turbulent boundary layer pressures. *Journal of Sound and Vibration* **206** (4), 541–565.
- Hwang, Yun Fan, Bonness, William K. & Hambric, Stephen A. 2003 On modeling structural excitations by low speed turbulent boundary layer flows. In *Technical Report 03-008*, p. 32.
- Mulchandani, Hiten, Adams, Melissa, Garcia-Mayoral, Ricardo, Vishwanathan, Vidya, Fritsch, Danny, Lowe, K T. & Devenport, William J. 2021 *Direct Numerical Simulations and Experiments of Turbulence Over Regular Roughness From the Transitionally Rough to the Fully Rough Regime*.
- Vishwanathan, Vidya, Fritsch, Daniel J., Lowe, K. Todd & Devenport, William J. 2023 History effects and wall-similarity of non-equilibrium turbulent boundary layers in varying pressure gradient over rough and smooth surfaces. *International Journal of Heat and Fluid Flow* **102**, 109145.